RSC Advances

PAPER

View Article Online
View Journal | View Issue



Cite this: *RSC Adv.*, 2019, **9**, 19641

# Efficient solid-state emission and reversible mechanofluorochromism of a tetraphenylethene-pyrene-based β-diketonate boron complex†

Ting Sun,[ab] Feng Zhao, *[ab] Gaolei Xi,[c] Jian Gong,[b] Mengyu Sun,[b] Chang Dong[b] and Jingyi Qiu[b]

Received 22nd May 2019
Accepted 10th June 2019

DOI: 10.1039/c9ra03847g

rsc.li/rsc-advances

A new twisted donor–acceptor (D–A) dye (**$BF_2$-TP**) that was composed of tetraphenylethene and pyrene connected with a β-diketonate boron moiety has been synthesized and characterized. Such a dye showed unique intramolecular charge transfer (ICT) features, which were evidenced by spectral analysis and theoretical calculations. More importantly, **$BF_2$-TP** solid samples exhibited an obvious mechanofluorochromic (MFC) behavior. Upon grinding with a spatula, the as-prepared powder sample illustrated a remarkable red shift of 62 nm, with considerable color contrast from yellow (562 nm) to orange red (624 nm). Its fluorescence color can be reversibly switched by repeating both the grinding–fuming and grinding–annealing processes. The mechanochromism is attributed to the phase transformation between amorphous and crystalline states. The results obtained would be helpful for designing novel MFC materials.

## Introduction

Mechanofluorochromic (MFC) dyes refer to a kind of "smart" material that exhibits tunable and switchable solid state fluorescence in response to mechanical stimuli including pressing, grinding, crushing, or rubbing, and can be reverted to the original state by recrystallization, thermal treatment, or exposure to solvent vapors.[1,2] Currently, these dyes have sparked tremendous interest owning to their unique properties and promising applications in the fields of optoelectronic devices,[3] mechanical sensors,[4] security ink,[5] rewritable media,[6] and fluorescent switches,[7] and so on. MFC dyes convert the fluorescence color *via* changing their chemical structure or aggregate morphology.[8] The former is a general method to alter the emission of a dye, but obtain limited success because of the irreversible and incomplete chemical reactions in the condensed phase. Most of the reported MFC dyes, the fluorescence color change are achieved through switch of their morphology under mechanical stimuli. These dyes can convert from crystal phase to amorphous state, or between two different crystalline phases upon modification of the intermolecular interactions, and produce a meta-stable state before and after the application of mechanical forces.[8a,9] Generally, the dyes possess nonplanar π-conjugated structures and hence afford a looser molecular packing pattern in the crystal states, and can be easily damaged under external stimuli. As is well known, the derivatives of tetraphenylethene,[6a,10] triphenylacrylonitrile,[11] triphenylamine,[12] and cyanoethylene,[13] as well as some boron complexes[14] are preferentially considered to act as MFC materials. Although the mechanisms for mechanochromism are somewhat clear, MFC dyes with extremely large MFC shifts (>60 nm) and obvious color contrast under simple mechanical force are still rare.[15] Lots of MFC materials, showing the MFC shifts within tens of nanometers, have been synthesized.[10a,14,16] MFC materials with bright solid-state emission and considerable color contrast are crucial for their usage in real world.[17] It is very important to rationally design and synthesize such new dyes with excellent MFC performances.

As one class of typical fluorescent dyes, β-diketonate boron complexes display impressive optical properties including high fluorescence quantum yields in the solution and in the solid states, large molar extinction coefficients, electron mobilities, and high electron affinities.[18,19] Therefore, they possess potential applications in laser dyes, imaging cells fluorophores, organic field effect transistors, and organic light emitting diodes (OLEDs).[20–23] Recent studies show that some β-diketonate boron complexes exhibited excellent MFC behavior, and numerous derivatives belonging to this family have been described. For example, Nguyen and co-workers[24] prepared a series of β-diketonate boron derivatives, and the photophysical properties of these dyes were reported to be related to the alkyl chains length. Gao *et al.*[25,26] synthesized a series of β-diketonate boron complexes, the excellent photoluminescence properties in the

[a]*School of Chemistry and Materials Science, Guizhou Education University, Guizhou 550000, P. R. China*

[b]*College of Chemistry and Chemical Engineering, Anyang Normal University, Anyang 455000, P. R. China. E-mail: zhaofeng@aynu.edu.cn*

[c]*Technology Ceter, China Tobacco Henan Industrial Co., Ltd., Zhengzhou 450000, P. R. China*

† Electronic supplementary information (ESI) available. See DOI: 10.1039/c9ra03847g

solid state and sensitive to mechanical forces can generally be observed. Usually, the dyes with moderate intramolecular charge transfer (ICT) properties exhibit high MFC capability. Moreover, it is worth mentioning that the extended π-conjugated dyes constructed by two π-conjugated structures intersecting at a β-diketonate boron core have recently attracted significant interest since their rigid π-conjugated skeletons bring a range of desired attributes. This phenomenon compelled us to explore novel MFC dyes based on β-diketonate boron complexes. In addition, pyrene derivatives are considered to be excellent luminogens due to their polarity sensitive vibronic emission, high charge carrier mobility, long fluorescence lifetime, chemical stability and also possessing large planar surface through effective π–π stacking between the molecules.[27] Herein, we designed and synthesized a novel D–A type MFC dye **$BF_2$-TP**, which composed of two chromophores of a pyrene unit and a tetraphenylethene moiety (Scheme 1). The steric hindrance comes from the two bulky substituents attaching on the central β-diketonate boron core endows the compound with a high torsional molecular conformation, resulting in effective inhibition of close π-packing and enhancement of emission quantum yields in the solid states. Results demonstrated that **$BF_2$-TP** gave strong emission in solution and in the solid state. In addition, **$BF_2$-TP** exhibit reversible mechanofluorochromic behavior upon the treatment of grinding/fuming or thermal annealing, and the emission color changed between yellow and orange red with large MFC shifts ($\Delta\lambda_{max}$ = 62 nm), showing a remarkable mechanochromism. These results are important for the development of novel MFC dyes that respond to mechanical stimulation, and extending the viability of MFC function into organic fluorescent materials.

# Experimental

### Materials and measurements

$^1$H and $^{13}$C NMR spectra were recorded on a Bruker-Avance 400 MHz spectrometer by using $CDCl_3$ as the solvents. Elemental analyses were performed with a PerkinElmer 240C elemental analyzer by investigation of C, H, and N. MS spectra were measured on Agilent Technologies 6224 spectrometer and MALDI-TOF MS Performance (Shimadzu, Japan). UV-visible spectra were carried out on a Shimadzu UV-2550 spectrophotometer. Fluorescence measurements were measured on a Cary Eclipse Fluorescence Spectrophotometer. The absolute fluorescence quantum yield for the solid sample was obtained using an Edinburgh FLS920 steady state spectrometer using an integrating sphere. Density functional theory (DFT) calculations were done employing the Gaussian 09W suit of programs at the B3LYP/6-31G(d) level. XRD patterns were measured on a Bruker D8 Focus Powder X-ray diffraction instrument.

### Synthesis

Tetrahydrofuran (THF) was dried over sodium and distilled under nitrogen immediately prior to use. Dichloromethane (DCM) was distilled under normal pressure over sodium hydride under nitrogen before use. The other chemicals were used as received without further purification. Column chromatography was carried out on silica (200–300 mesh). Compounds **3** and **5** were synthesized according to the literatures.[25,28]

The synthetic routes for β-diketonate boron complex **$BF_2$-TP** were shown in Scheme 2. Firstly, the tetraphenylethene derivative **3** was synthesized by Suzuki–Miyaura coupling between **1** and boric acid **2**. Then the key intermediate **6** was obtained through the Friedel–Crafts alkylation reaction and the next Friedel–Crafts acyl reaction by using pyrene **4** as the starting material. Finally, the target molecules **$BF_2$-TP** was prepared between **3** and **6** in the presence of sodium hydride in anhydrous THF followed by complexation with boron trifluoride diethyl etherate, to give a yield of 62%. **$BF_2$-TP** has good solubility in common organic solvents such as THF, DCM, chloroform, and toluene, but show poor solubility in aliphatic hydrocarbon solvents (such as cyclohexane and *n*-hexane) and protic solvents (such as methanol and ethanol). The intermediates and the final products have been carefully purified and fully characterized by $^1$H and $^{13}$C NMR, MALDI-TOF mass spectrometry, and C, H, N elemental analyses.

### 1-(2,7-Di-*tert*-butylpyren-4-yl)ethanone (6)

$AlCl_3$ (12.2 g, 91.8 mmol) is added in 1,2-dichloroethane (100 mL) followed by the addition of acetyl chloride (7.2 g, 91.8 mmol) slowly over 30 min at 5 °C. Compound **5** (9.42 g, 30.0 mmol) in 1,2-dichloroethane (40 mL) was then added slowly, and the reaction mixture was stirred for 2 h at room temperature and kept for 2 h at 35 °C. Then the mixture was cooled to room

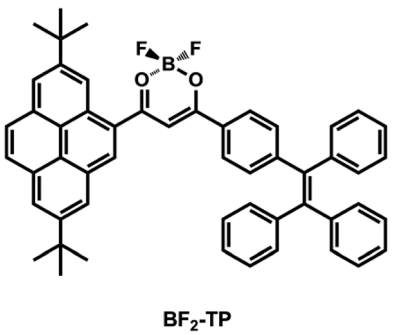


Scheme 1 The molecular structure of $BF_2$-TP.

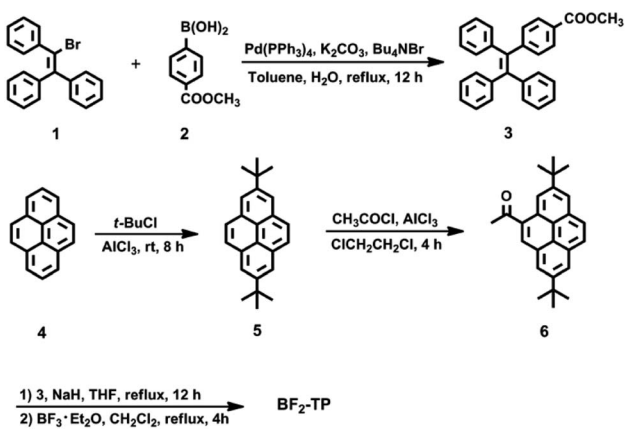


Scheme 2 Synthetic routes of $BF_2$-TP.

temperature and the solvent was removed under reduced pressure. An orange solid appeared after dilute HCl (200 mL) was added to the flask. The solid is filtered and washed with water, followed by recrystallization from ethanol to give a white solid (9.63 g). Yield 90% mp 133.0–135.0 °C. $^1$H NMR (400 MHz, $CDCl_3$) $\delta$ 9.25 (s, 1H), 8.61 (s, 1H), 8.30–8.25 (m, 3H), 8.08–8.01 (m, 2H), 2.96 (s, 3H), 1.61 (s, 18H) (Fig. S3†); $^{13}$C NMR (100 MHz, $CDCl_3$) $\delta$ 201.93, 149.50, 149.06, 134.73, 132.37, 130.78, 128.89, 128.33, 127.12, 126.69, 124.53, 123.90, 123.66, 123.52, 122.93, 121.88, 35.50, 35.22, 31.94, 31.88, 29.92 (Fig. S4†); TOF LC/MS: *m*/*z*: calculated for $C_{26}H_{28}O$: 356.2140; found: 356.2132 (Fig. S5†). Anal. calcd. for $C_{28}H_{22}O$: C 87.60, H 7.92; found: C 87.71, H 7.83.

### 6-(2,7-Di-*tert*-butylpyren-4-yl)-2,2-difluoro-4-(4-(1,2,2-triphenylvinyl)phenyl)-2*H*-1,3,2-dioxaborinin-1-ium-2-uide ($BF_2$-TP)

A mixture of **3** (2.00 g, 5.13 mmol) and **6** (1.66 g, 4.66 mmol) was dissolved in dry THF (80 mL), and then NaH (60%, 1.03 g, 25.75 mmol) was added. Under an atmosphere of nitrogen, the mixture was refluxed with stirring for 24 h. After the reaction was over, the mixture was cooled to room temperature. And then the mixture was acidified with dilute HCl and extracted with DCM. After solvent removal, the solid residue was dried under vacuum. The obtained solid was dissolved in dry DCM (80 mL), and boron trifluoride diethyl etherate (2.95 mL, 3.31 g, 23.30 mmol) was added to the solution. The mixture was stirred for 24 h under an atmosphere of nitrogen at room temperature. Then the mixture was poured into the water, and extracted with DCM. After solvent removal, the crude product was purified by column chromatography (silica gel, DCM/petroleum ether, v/v = 2/3), affording a yellowish green solid (2.31 g). Yield 65%. $^1$H NMR (400 MHz, $CDCl_3$) $\delta$ 8.94 (s, 1H), 8.65 (s, 1H), 8.34 (d, $J$ = 5.2 Hz, 2H), 8.29 (s, 1H), 8.10–8.04 (m, 2H), 7.98 (d, $J$ = 8.4 Hz, 2H), 7.25 (d, $J$ = 8.4 Hz, 3H), 7.18–7.15 (m, 9H), 7.06 (s, 6H), 1.60 (s, 9H), 1.59 (s, 9H) (Fig. S6†); $^{13}$C NMR (100 MHz, $CDCl_3$) $\delta$ 186.69, 182.30, 151.96, 149.65, 149.50, 143.91, 142.88, 142.64, 139.50, 133.17, 132.20, 131.33, 131.23, 131.09, 129.65, 128.73, 128.54, 128.27, 128.05, 127.77, 127.33, 127.05, 126.62, 125.45, 124.34, 123.43, 121.09, 98.10, 35.54, 35.27, 31.84 (Fig. S8†). HRMS (MALDI-TOF) *m*/*z*: $[M + H]^+$ calcd. for $C_{53}H_{46}BF_2O_2$: 763.3559; found: 763.7036 (Fig. S9†). Anal. calcd. for $C_{53}H_{45}BF_2O_2$: C 83.46, H 5.95; found: C 83.54, H 5.81.

### Preparation of the samples for mechanofluorochromism study

The grinding powders were obtained by grinding the as-prepared powder with a pestle in the mortar. The fumed samples were prepared by fuming the grinding powder with DCM for 2 min. The annealing samples were obtained by heating the ground powders at 200 °C for 5 min.

## Result and discussion

### Absorption and fluorescence studies

Optical properties of the compound **$BF_2$-TP** in solvents with different polarities was investigated by UV-vis and fluorescence spectroscopy. The UV-vis absorption and fluorescence emission spectra are demonstrated in Fig. 1, and the corresponding photophysical data are summarized in Table S1.† From the UV-vis absorption spectra (Fig. 1a), a relative strong absorption band at $\lambda$ = 280–360 nm was attributed to $\pi$–$\pi$* local electron transitions of the conjugate system, which did not shift with increasing polarity of the deduced from the solvent-dependent absorption spectra. For example, in hexane, the CT band of **$BF_2$-TP** centered at 411 nm and red-shifted gradually with increasing solvent polarity, its emission band reached 429 nm in DMSO. Form the fluorescence spectra (Fig. 1b), along with

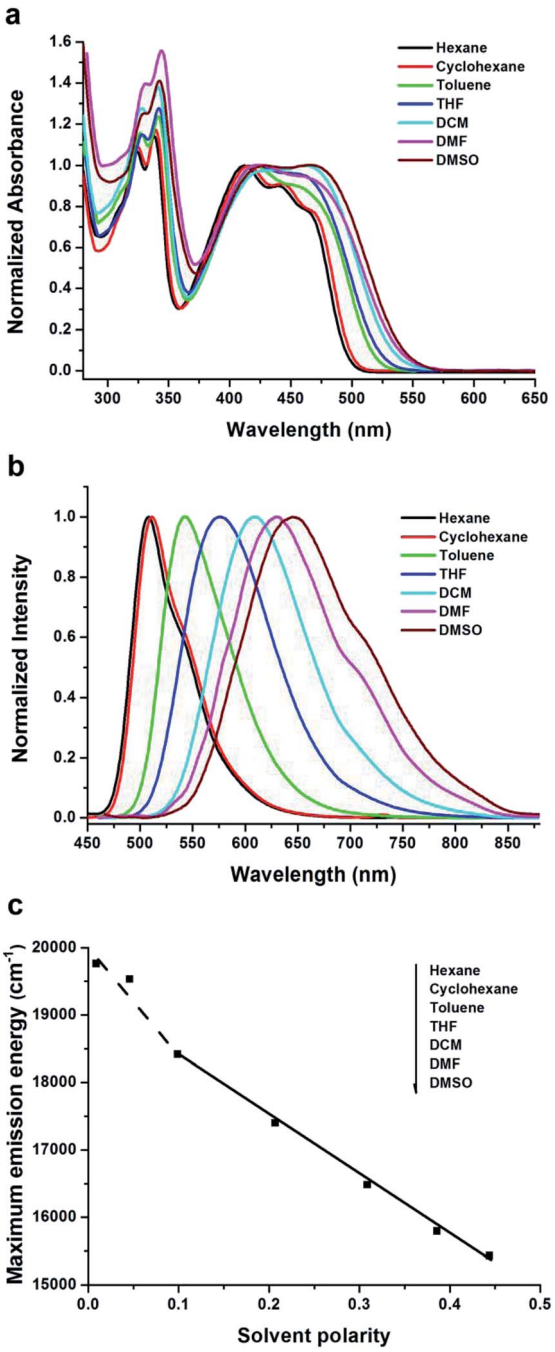


Fig. 1 Normalized UV-vis absorption (a) and PL (b, $\lambda_{ex}$ = 420 nm) spectra of $BF_2$-TP in different solvents ($1.0 \times 10^{-5}$ mol L$^{-1}$). (c) Lippert–Mataga plot: fluorescence emission maximum energy of $BF_2$-TP as a function of solvent polarity.

the increase of the polarity of the solvent, the emission bands of **$BF_2$-TP** red-shifted rapidly and became broad. In the same time, the large Stokes shift is also observed. For example, **$BF_2$-TP** emitted blue light appeared at 507 nm in hexane and green light located at 645 nm in DMSO with the band broadening, and was accompanying with large Stokes shift from 4548 $cm^{-1}$ in hexane to 7806 $cm^{-1}$ in DMSO. Combining the obvious transition to the low-energy direction, the significant Stokes shifts, and the extension of the emission bands indicated that ICT transitions of **$BF_2$-TP** take place in polar solvents.[29] It should be mentioned that the fluorescence spectra of **$BF_2$-TP** exhibited vibrational structures in non-polar solvents, such as hexane and cyclohexane, which recommends two separated close-lying excited states. This phenomenon suggests that the locally excited (LE) state is responsible for the emission of **$BF_2$-TP** in nonpolar solvents.[30] The effects of solvents on the emission features can be further evaluated by the relationship between the emission maximum energy and a function of the Lippert solvent polarity (Lippert–Mataga). It illustrated the conformational change of the excited state surface prior to the emission.[31] As shown in Fig. 1c, the slope can be used to assess the change in dipole moment upon excitation, and the break in the linear relationship suggests the existence of two different excited states. The deviation of the emission maximum energy in cyclohexane and hexane from the linear relationship followed by those in other solvents are in support of the fact that the emission of **$BF_2$-TP** origins from the LE state in non-polar solvents, and from the ICT state in polar solvents.[32] Moreover, the fluorescence quantum yield ($\Phi_f$) of **$BF_2$-TP** (Table S1†) showed a notable decrease with the increasing solvent polarity. The $\Phi_f$ value was from 0.369 to 0.083 when the solvent was changed from apolar (*e.g.*, hexane) to highly polar (*e.g.*, DMSO), further confirming unique ICT nature of compound **$BF_2$-TP**.

To gain a better insight into optical properties of **$BF_2$-TP**, density functional theory (DFT) calculations was performed at the B3LYP/6-31G(d) level basis in the Gaussian 09W program package. As shown in Fig. 2, the HOMO is delocalized on the *tert*-butyl substituted pyrene fragment, while the LUMO is mainly distributed over the dioxaborine ring, as well as the tetraphenylethylene group. Thus, it can be inferred from the orbital distribution pattern that ICT occurs largely from the *tert*-butyl substituted pyrene unit to the dioxaborine ring regardless of whether tetraphenylethylene was present as a competing donor unit. In addition, the geometry optimized structures of **$BF_2$-TP** demonstrate highly twisted spatial conformation. The dihedral angles between *tert*-butyl substituted pyrene (B) and the dioxaborine ring (C) is 43.7°, and the dihedral angles between the side benzene rings (A) in tetraphenylethene and the dioxaborine ring (C) is 16.9°. Such torsional angles in **$BF_2$-TP** will prevent the molecules from packing in a close π–π stacking mode in the solid state and thus may endow it with MFC feature.

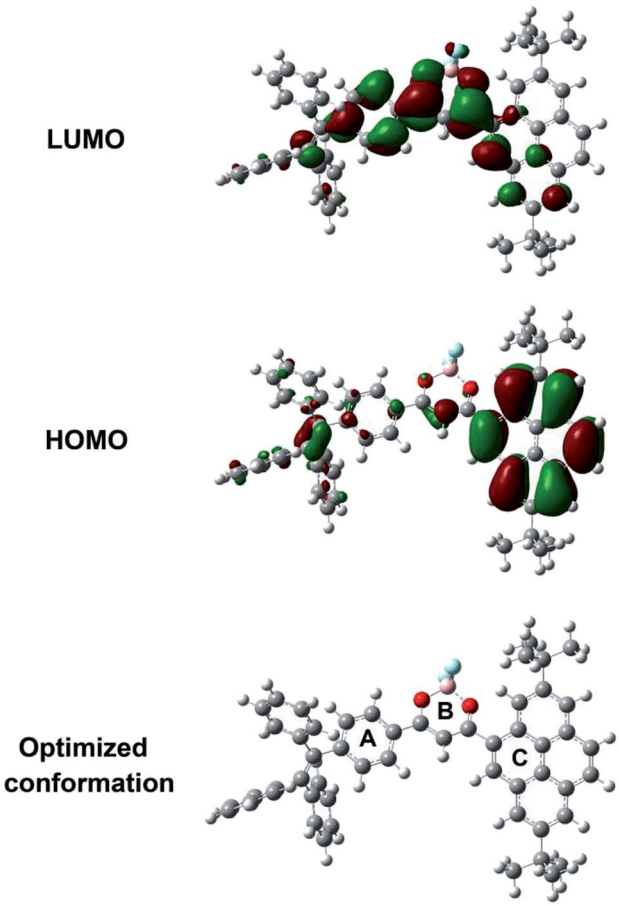


Fig. 2 The frontier orbital contributions of $BF_2$-TP calculated by DFT in Gaussian 09 at the B3LYP/6-31G(d) level.

## Mechanofluorochromic properties

The crude product was purified on a silica-gel column to afford an orange powder. The **$BF_2$-TP** powder demonstrated strong yellow emissions under 365 nm UV-light illumination, the quantum efficiencies of the as-prepared solid states was 0.46. Interestingly, after grinding with a mortar and pestle, the powder changed its emission color into orange red, demonstrating a property of mechanochromic fluorescence. After exposure to the vapor of DCM for 2 min, the emission color of the ground powder changed back to initial yellow and the as-prepared powder was obtained again. The mechano-fluorochromic process is reproducible, which meant that the fluorescence transformation between yellow and orange red is reversible switched. As shown in Fig. S1,† the dye displayed excellent reversibility with almost no fatigue in response throughout the six cycles. The PL spectra measurement was applied to monitor such a reversible color switching under external stimuli. As depicted in Fig. 3a, the emission spectrum of **$BF_2$-TP** is obvious with the initial emission centered at $\lambda_{max}$ 562 nm shifting to 624 nm after the mechanical grinding; that is, a spectral red-shift of 62 nm occurred simply by grinding. After fuming treatment, the emission peak of the ground solid blue-shifted to the initial wavelength. It is noted that the vapor fuming progress can be replaced by thermal annealing. When the ground sample of **$BF_2$-TP** is annealed at 200 °C for 5 min, it could recover to the emission color of the original state corresponding as-prepared sample. At the same time, the recovery of the emission spectrum of **$BF_2$-TP** could also be observed by heating its ground sample.

 

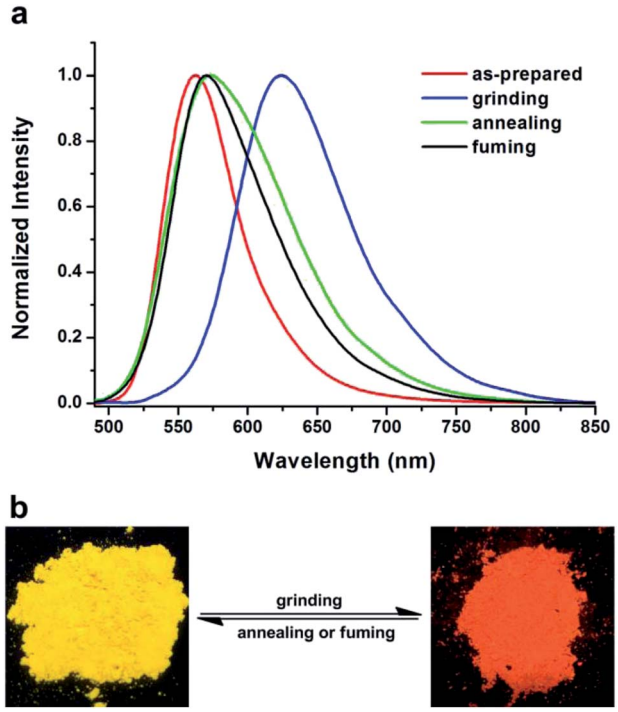


Fig. 3 (a) Normalized fluorescent spectra of $BF_2$-TP in different solid-states: as-synthesized, grinding and fuming, $\lambda_{ex} = 370$ nm. (b) Photos of $BF_2$-TP color changes under grinding and fuming stimuli.

The experiment of time-resolved fluorescence was carried out (Fig. S2a†) and the corresponding data are illustrated in Table S2.† The fluorescence decay curves were fitted by a double-exponential decay for **$BF_2$-TP** in solid states, which revealed the mixture of two distinguished emission states in the amorphous phase. The fluorescent lifetime of ground sample and as-prepared sample were 7.57 ns and 3.61 ns, respectively. The longer lifetime of 7.57 ns indicted the formation of excimers after pressing.

Switchable mechanochromic dye of **$BF_2$-TP** with a large shift of 62 nm prompts us to evaluate it as a kind of smart material with numerous potential applications. An example of such applications is demonstrated in Fig. 4, after being simply pressed by streaking a metal spatula on a piece filter paper with sprayed as-synthesized powder, an orange red letter appeared on the yellow background due to the amorphization of **$BF_2$-TP** in the written "A" area under UV light illumination (Fig. 4b). Interestingly, after thermal annealing or vapor fuming the letter "A" can be merged in the background because of the crystallization of **$BF_2$-TP** in area of "A" (Fig. 4c), and the clear orange red letter "B" can be written again (Fig. 4d). Such writing and erasing process can be repeated many times through repeating writing and fuming processes. The letters are invisible under room lighting but become visible with UV illumination. On the basis of its excellent MFC properties, **$BF_2$-TP** may be utilized as optical recording materials.

With the aim of getting insight into the mechano-induced emission color changes, powder X-ray diffraction (XRD) was used to study the crystalline states (Fig. 5a). Many sharp and intense reflection peaks were observed in the diffraction pattern

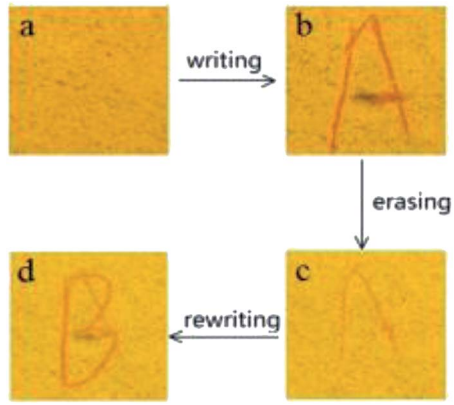


Fig. 4 Photos of the luminescence writing/erasing process of $BF_2$-TP on filter papers under 365 nm UV light illumination: (a) fluorescence emission of as-prepared powder; (b) the letter of "A" was written with a spatula; (c) the paper was erased by vapor fuming or thermal annealing; (d) rewritable the letter of "B" generated with a spatula.

of the untreated sample, indicating that the as-prepared **$BF_2$-TP** is well-ordered arrangement crystalline structure. In sharp contrast, all of the diffraction peaks displays diffuse and depressed reflections after grinding, verifying that the ground

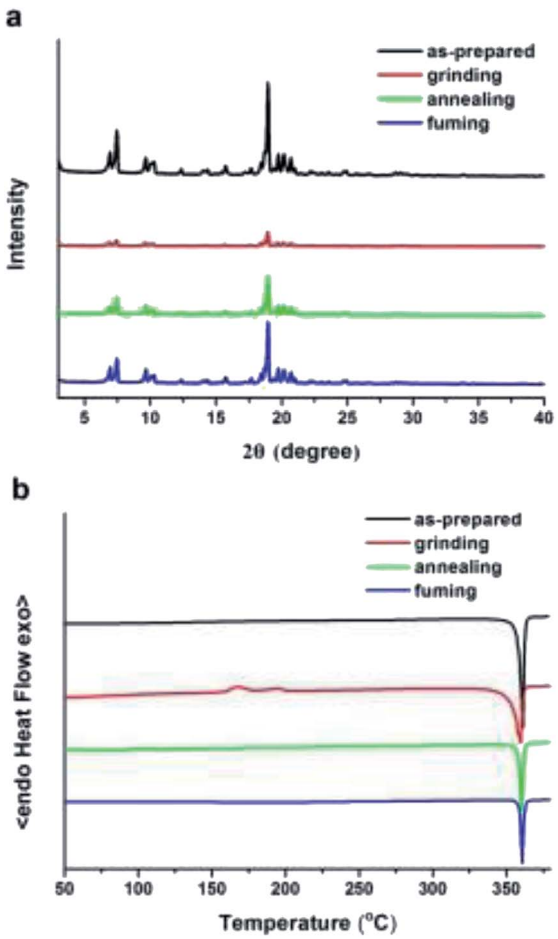


Fig. 5 (a) XRD patterns of $BF_2$-TP in different solid states: as-prepared, grinding, annealing and fuming. (b) DSC curves of $BF_2$-TP in the ground and the crystalline states.

sample is amorphous. Furthermore, when fumed with DCM or annealed, sharp reflection peaks resemble to those of the as prepared powder emerge out, suggesting the ground sample can be readily converted back into an ordered crystalline lattice. Accordingly to these results, the mechanochromism of **$BF_2$-TP** should be attributed to the crystalline–amorphous phase transformations, which greatly influences photophysical properties. Analysis by differential scanning calorimetry (DSC) also substantiates the above claim, and the results are presented in Fig. 5b. The as-prepared sample of **$BF_2$-TP** demonstrated a strong endothermic peak at 362 °C, which corresponded to its melt point. After grinding, there are two cold-crystallization transition peaks at 167.0 °C and 195.0 °C before melting, indicating that a metastable aggregation structure in the ground sample is produced, and it would transfer to the more-stable state. After treatment by annealing at 200 °C for 5 min or solvent fuming by DCM for 2 min, the cold-crystallization transitions vanish and the shapes of the DSC curve is very similar to that obtain from the as-prepared sample. These results further confirm that the grinding treatment causes the transition in morphology of **$BF_2$-TP**, meanwhile, the morphology transition can easily be recovered through fuming or annealing treatment.

## Conclusion

In this work, a novel D-A structured compound **$BF_2$-TP** showing typical ICT characteristics has been successfully obtained and potential application of **$BF_2$-TP** has also been investigated. The emission color of **$BF_2$-TP** powders changed from initial yellow to final orange red under simple mechanical force, accompanied with the remarkable spectral shift of 62 nm. Moreover, the spectroscopic properties and morphological structures of the solid **$BF_2$-TP** can be smartly switched in the grinding-heating or grinding–fuming fluorochromic process. The result indicates that the MFC behavior of **$BF_2$-TP** is attributed to the reversible phase transformation between crystal and amorphous states. Thus, these intriguing properties enable **$BF_2$-TP** for various potential applications in security inks, rewritable sensors, and light-emitting devices.

## Conflicts of interest

There are no conflicts to declare.

## Acknowledgements

We are grateful to the Program for Innovative Research Team of Science and Technology in the University of Henan Province (18IRTSTHN004), and Anyang Normal University Program (AYNU-2017-B16, AYNUKP-2018-B20) for financial support of this research.

## Notes and references

1 (*a*) K. M. Wiggins, J. N. Brantley and C. W. Bielawski, *Chem. Soc. Rev.*, 2013, **42**, 7130–7147; (*b*) Z. G. Chi, X. Q. Zhang, B. Q. Xu, X. Zhou, C. P. Ma, Y. Zhang, *et al.*, *Chem. Soc. Rev.*, 2012, **41**, 3878–3896; (*c*) Y. Wang, M. J. Li, Y. M. Zhang, J. Yang, S. Y. Zhu, L. Sheng, *et al.*, *Chem. Commun.*, 2013, **49**, 6587–6589; (*d*) X. Q. Zhang, Z. G. Chi, B. J. Xu, C. J. Chen, X. Zhou, Y. Zhang, *et al.*, *J. Mater. Chem.*, 2012, **22**, 18505–18513.

2 (*a*) F. Ciardelli, G. Ruggeri and A. Pucci, *Chem. Soc. Rev.*, 2013, **42**, 857–870; (*b*) R. Misra, T. Jadhav, B. Dhokale and S. M. Mobin, *Chem. Commun.*, 2014, **50**, 9076–9078; (*c*) N. Mizoshita, T. Tani and S. Inagaki, *Adv. Mater.*, 2012, **24**, 3350–3355; (*d*) H. Zhang, F. Gao, X. D. Cao, Y. Q. Li, Y. Z. Xu, W. G. Weng, *et al.*, *Angew. Chem., Int. Ed.*, 2016, **55**, 3040–3044; (*e*) C. P. Ma, B. J. Xu, G. Y. Xie, J. J. He, X. Zhou, B. Y. Peng, *et al.*, *Chem. Commun.*, 2014, **50**, 7374–7377; (*f*) K. Ohno, S. Yamaguchi, A. Nagasawa and T. Fujihara, *Dalton Trans.*, 2016, **45**, 5492–5503; (*g*) S. S. Zhao, L. Chen, L. Wang and Z. G. Xie, *Chem. Commun.*, 2017, **53**, 7048–7051; (*h*) H. W. Wu, C. Hang, X. Li, L. Y. Yin, M. J. Zhu, J. Zhang, *et al.*, *Chem. Commun.*, 2017, **53**, 2661–2664.

3 (*a*) C. L. Li, S. P. Wang, W. P. Chen, J. B. Wei, G. C. Yang, K. Q. Ye, *et al.*, *Chem. Commun.*, 2015, **51**, 10632–10635; (*b*) C. L. Li, J. B. Wei, J. X. Han, Z. Q. Li, X. X. Song, Z. L. Zhang, *et al.*, *J. Mater. Chem. C*, 2016, **4**, 10120–10129.

4 (*a*) A. Facchetti, *Chem. Mater.*, 2010, **23**, 733–758; (*b*) J. Mei, J. Wang, J. Z. Sun, H. Zhao, W. Z. Yuan, C. M. Deng, *et al.*, *Chem. Sci.*, 2012, **3**, 549–558; (*c*) S. Pagidi and P. Thilagar, *J. Mater. Chem. C*, 2017, **5**, 6537–6546.

5 (*a*) S. Sasaki, G. P. C. Drummen and G. Konishi, *J. Mater. Chem. C*, 2016, **4**, 2731–2743; (*b*) Y. Yuan, W. Yuan and Y. Chen, *Sci. China Mater.*, 2016, **59**, 507–520.

6 (*a*) Q. Y. Lu, X. F. Li, J. Li, Z. Y. Yang, B. J. Xu, Z. G. Chi, *et al.*, *J. Mater. Chem. C*, 2015, **3**, 1225–1234; (*b*) X. L. Luo, J. N. Li, C. H. Li, L. P. Heng, Y. Q. Dong, Z. P. Liu, *et al.*, *Adv. Mater.*, 2011, **23**, 3261–3265; (*c*) C. Li, X. Luo, W. Zhao, Z. Huang, Z. Liu, B. Tong, *et al.*, *Sci. China: Chem.*, 2013, **56**, 1173–1177.

7 (*a*) Z. Ma, M. Teng, Z. Wang, S. Yang and X. Jia, *Angew. Chem., Int. Ed.*, 2013, **52**, 12268–12272; (*b*) X. Cheng, D. Li, Z. Zhang, H. Zhang and Y. Wang, *Org. Lett.*, 2014, **16**, 880–883; (*c*) Y. Shi, Y. Cai, Y. J. Wang, M. Chen, H. Nie, W. Qin, *et al.*, *Sci. China: Chem.*, 2017, **60**, 635–641.

8 (*a*) Y. Sagara, T. Mutai, I. Yoshikawa and K. Araki, *J. Am. Chem. Soc.*, 2007, **129**, 1520–1521; (*b*) D. A. Davis, A. Hamilton, J. L. Yang, L. D. Cremar, G. D. Van, S. L. Potisek, *et al.*, *Nature*, 2009, **459**, 68–72; (*c*) K. Wang, H. Zhang, S. Chen, G. Yang, J. Zhang, W. Tian, *et al.*, *Adv. Mater.*, 2014, **26**, 6168–6173; (*d*) K. Ariga, T. Mori and J. P. Hill, *Adv. Mater.*, 2012, **24**, 158–176; (*e*) S. J. Yoon, J. W. Chung, J. Gierschner, K. S. Kim, M. G. Choi, D. Kim, *et al.*, *J. Am. Chem. Soc.*, 2010, **132**, 13675–13683.

9 (*a*) Y. Ooyama, Y. Kagawa, H. Fukuoka, G. Ito and Y. Harima, *Eur. J. Org. Chem.*, 2009, **2009**, 5321–5326; (*b*) S. J. Yoon and S. Park, *J. Mater. Chem.*, 2011, **21**, 8338–8346.

10 (*a*) X. Y. Shen, Y. J. Wang, E. Zhao, W. Z. Yuan, Y. Liu, P. Lu, *et al.*, *J. Phys. Chem. C*, 2013, **117**, 7334–7347; (*b*) J. H. Jia, P. C. Xue and R. Lu, *Tetrahedron Lett.*, 2016, **57**, 2544–2548; (*c*) J. Shi, W. Zhao, C. Li, Z. Liu, Z. Bo, Y. Dong, *et al.*, *Chin.*

 

*Sci. Bull.*, 2013, **58**, 2723–2727; (*d*) M. P. Aldred, G. F. Zhang, C. Li, G. Chen, T. Chen and M. Q. Zhu, *J. Mater. Chem. C*, 2013, **1**, 6709–6718; (*e*) H. Gao, D. Xu, X. Liu, A. Han, L. Zhou, C. zhang, *et al.*, *RSC Adv.*, 2017, **7**, 1348–1356.

11 (*a*) Y. Gong, Y. Tan, J. Liu, P. Lu, C. Feng, W. Z. Yuan, *et al.*, *Chem. Commun.*, 2013, **49**, 4009–4011; (*b*) W. Z. Yuan, Y. Q. Tan, Y. Y. Gong, P. Lu, J. W. Y. Lam, X. Y. Shen, *et al.*, *Adv. Mater.*, 2013, **25**, 2837–2843.

12 (*a*) L. Zhou, D. Xu, H. Gao, A. Han, X. Liu, C. Zhang, *et al.*, *Dyes Pigm.*, 2017, **137**, 200–207; (*b*) Q. Q. Fang, Q. Wang, W. Lin, X. Yu, Y. Q. Dong and Y. W. Chi, *Sens. Actuators, B*, 2017, **244**, 771–776.

13 J. Zhao, Z. Chi, Y. Zhang, Z. Mao, Z. Yang, E. Ubba, *et al.*, *J. Mater. Chem. C*, 2018, **6**, 6327–6353.

14 J. Zhao, J. Peng, P. Chen, H. Wang, P. Xue and R. Lu, *Dyes Pigm.*, 2018, **149**, 276–283.

15 (*a*) A. Balch, *Angew. Chem., Int. Ed.*, 2009, **48**, 2641–2644; (*b*) Y. J. Dong, B. Xu, J. B. Zhang, X. Tan, L. J. Wang, J. L. Chen, *et al.*, *Angew. Chem., Int. Ed.*, 2012, **51**, 10782–10785; (*c*) Y. Zhang, K. Wang, G. Zhuang, Z. Xie, C. Zhang, F. Cao, *et al.*, *Chem.–Eur. J.*, 2015, **21**, 2474–2479; (*d*) W. Liu, S. Ying, Q. Sun, X. Qiu, H. Zhang, S. Xue, *et al.*, *Dyes Pigm.*, 2016, **125**, 8–14.

16 (*a*) Y. Zhao, H. Lin, M. Chen and D. Yan, *Ind. Eng. Chem. Res.*, 2014, **53**, 3140–3147; (*b*) Y. Li, Z. Zhuang, G. Lin, Z. Wang, P. Shen, Y. Xiong, *et al.*, *New J. Chem.*, 2018, **42**, 4089–4094; (*c*) M. Chen, R. Chen, Y. Shi, J. Wang, Y. Cheng, Y. Li, *et al.*, *Adv. Funct. Mater.*, 2018, **28**, 1704689; (*d*) C. Lin, Y. Liu, S. Peng, T. Shinmyozu and J. Yang, *Inorg. Chem.*, 2017, **56**, 4978–4989.

17 (*a*) T. Han, X. Feng, D. Chen and Y. Dong, *J. Mater. Chem. C*, 2015, **3**, 7446–7454; (*b*) Y. Q. Dong, J. W. Lam and B. Z. Tang, *J. Phys. Chem. Lett.*, 2015, **6**, 3429–3436; (*c*) X. Hou, C. Ke, C. J. Bruns, P. R. McGonigal, R. B. Pettman and J. F. Stoddart, *Nat. Commun.*, 2015, **6**, 6884; (*d*) F. Xu, T. Nishida, K. Shinohara, L. Peng, M. Takezaki, T. Kamada, *et al.*, *Organometallics*, 2017, **36**, 556–563.

18 T. D. Liu, A. D. Chien, J. W. Lu, G. Q. Zhang and C. L. Fraser, *J. Mater. Chem.*, 2011, **21**, 8401–8408.

19 G. Zhang, J. Lu, M. Sabat and C. L. Fraser, *J. Am. Chem. Soc.*, 2010, **132**, 2160–2162.

20 (*a*) H. Maeda, Y. Mihashi and Y. Haketa, *Org. Lett.*, 2008, **10**, 3179–3182; (*b*) K. Ono, K. Yoshikawa, Y. Tsuji, H. Yamaguchi, R. Uozumi, M. Tomura, *et al.*, *Tetrahedron*, 2007, **63**, 9354–9358; (*c*) E. Cogne-Laage, J. F. Allemand, O. Ruel, J. B. Baudin, V. Croquette, M. Blanchard-Desce, *et al.*, *Chem.–Eur. J.*, 2004, **10**, 1445–1455.

21 G. Zhang, J. Chen, S. J. Payne, S. E. Kooi, J. N. Demas and C. L. Fraser, *J. Am. Chem. Soc.*, 2007, **129**, 8942–8943.

22 (*a*) A. Nagai, K. Kokado, Y. Nagata, M. Arita and Y. Chujo, *J. Org. Chem.*, 2008, **73**, 8605–8607; (*b*) A. Nagai, K. Kokado, Y. Nagata and Y. Chujo, *Macromolecules*, 2008, **41**, 8295–8298.

23 (*a*) J. Fabian and H. Hartmann, *J. Phys. Org. Chem.*, 2004, **17**, 359–369; (*b*) B. Domercq, C. Grasso, J. L. Maldonado, M. Halik, S. Barlow, S. R. Marder, *et al.*, *J. Phys. Chem. B*, 2004, **108**, 8647–8651; (*c*) Y. Sun, D. Rohde, Y. Liu, L. Wan, Y. Wang, W. Wu, *et al.*, *J. Mater. Chem.*, 2006, **16**, 4499–4503.

24 N. D. Nguyen, G. Q. Zhang, J. W. Liu, A. E. Sherman and C. L. Fraser, *J. Mater. Chem.*, 2011, **21**, 8409–8415.

25 H. Gao, D. Xu, X. Liu and A. Han, *Dyes Pigm.*, 2017, **139**, 157–165.

26 H. Gao, D. Xu, Y. Wang, Y. Wang, X. Liu, A. Han, *et al.*, *Dyes Pigm.*, 2018, **150**, 59–66.

27 (*a*) A. Kathiravan, K. Sundaravel, M. Jaccob, G. Dhinagaran, A. Rameshkumar, D. Arul Ananth, *et al.*, *J. Phys. Chem. B*, 2014, **118**, 13573–13581; (*b*) M. Shellaiah, Y. H. Wu, A. Singh, M. V. R. Raju and H. C. Lin, *J. Mater. Chem. A*, 2013, **1**, 1310–1318.

28 Z. Wu, Z. Huang, R. Guo, C. Sun, L. Chen, B. Sun, *et al.*, *Angew. Chem., Int. Ed.*, 2017, **56**, 13031–13035.

29 J. S. Yang, K. L. Liau, C. M. Wang and C. Y. Hwang, *J. Am. Chem. Soc.*, 2004, **126**, 12325–12335.

30 G. Jones II, W. R. Jackson, C. Choi and W. R. Bergmark, *J. Phys. Chem.*, 1985, **89**, 294–300.

31 C. Reichardt, *Chem. Rev.*, 1994, **94**, 2319–5238.

32 F. Loiseau, S. Campagna, A. Hameurlaine and W. Dehaen, *J. Am. Chem. Soc.*, 2005, **127**, 11352–11363.